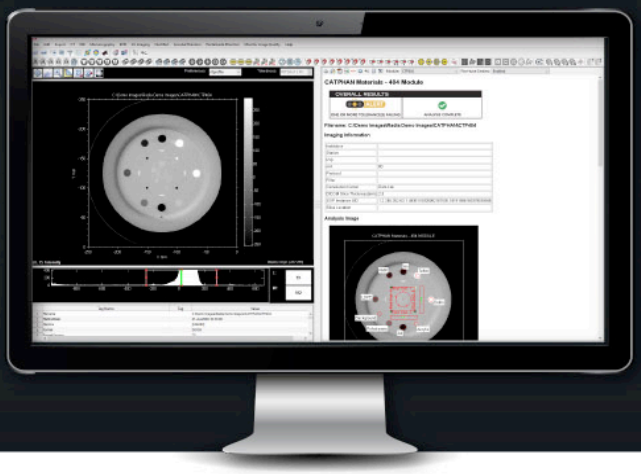

Radia therapy

Radia is an à la carte-based software for comprehensive imaging QA/QC at your facility. Easily customize your Radia software by adding the therapy modules needed to perform automated analyses on your facility's phantoms.

Radia is tailored specifically for you. Select and purchase any of the modules listed below to create a customized software package for your imaging QA needs. RIT provides fast, robust, and accurate analysis of all imaging tests recommended in TG-142. Easily automate your LINAC image QA and get quantitative, repeatable analysis for all tests. Full reports of all imaging tests are easily generated, and results can be automatically tracked with RIT*trend*™.

THERAPY MODULES & PHANTOMS

ACR MR Module

- ACR Large MR Phantom

ACR CT Module

- ACR CT Phantom

ISOCube Module

- Standard Imaging ISOCube Phantom

Penta-Guide Module

- Modus (IBA) Penta-Guide Phantom

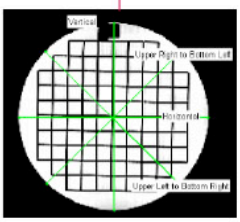

Catphan/OBI Module

- CATPHAN® 500/600 Series Phantom
- Elekta 503 CATPHAN® (XVI) Phantom
- Varian 504 & 604 CATPHAN® Phantom
- Siemens MV CT (OBI) Phantom

Electron Density/Tissue Characterization Module

- Accuray TomoTherapy® Cheese MVCT Phantom
- CIRS CT Phantoms: 062, 062A, 062M (Cone Beam)
- Gammex 467 CT Phantom

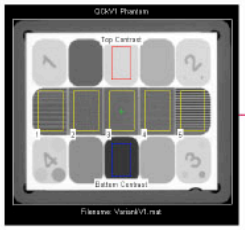

kV Imaging Module

- IBA Primus®-L Phantom
- Leeds TOR 18FG Phantom
- PTW NORMI® 4 Phantom (20 x 20 cm and 30 x 30 cm)
- Standard Imaging QCkV-1 Phantom

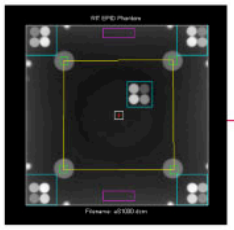

EPID MV Imaging Module

- RIT EPID Phantom (EPID QA Phantom, manufactured & sold by Standard Imaging)
- PTW EPID QC Phantom
- Las Vegas EPID Phantoms
- Standard Imaging QC-3 Phantom

AUTOMATION & CUSTOMIZATION FEATURES

Hands-Free Automation

Use Cerberus to perform hands-free, fully automated phantom analysis. Cerberus automatically monitors folders, selects files based on your criteria, and analyzes them in the background of your machine.

Batch Image Analysis

Use the RunQueueC Image Sequencer to perform one-click batch analysis on any number of images queued into the system. In seconds, each image slice of the phantom is analyzed automatically and the results exported to your preferred format.

Tracking and Trending

RIT*trend*™ is the all-in-one statistical database solution for all of your department's measurements. Export full reports of all imaging tests with a single click and trend results over time.

Tolerance Customization

RIT's Tolerance Manager sets tolerance values and pass/fail criteria for every measurement. Preference profiles can be precisely curated to each individual machine in use.

RIT®

CLICK TO VISIT **RADIMAGE.COM** TO DEMO RIT'S ADVANCED RANGE OF MACHINE QA, MLC QA, PATIENT QA, AND IMAGING QA ROUTINES.

+1(719)590-1077, OPT. 4

SALES@RADIMAGE.COM

© 2023, Radiological Imaging Technology, Inc.

RIT*trend*™ is a trademark of Radiological Imaging Technology, Inc. CATPHAN® is a registered trademark of The Phantom Laboratory. NORMI® is a registered trademark of PTW. Primus® is a registered trademark of IBA. ISOCube™ is a trademark of IMT, Inc.

In vivo accuracy assessment of a needle-based navigation system for CT-guided radiofrequency ablation of the liver

Lena Maier-Hein[a)]
Division of Medical and Biological Informatics, German Cancer Research Center, Im Neuenheimer Feld 280, 69120 Heidelberg, Germany

Aysun Tekbas
Department of General, Abdominal and Transplant Surgery, University of Heidelberg, Im Neuenheimer Feld 110, 69120 Heidelberg, Germany

Alexander Seitel
Division of Medical and Biological Informatics, German Cancer Research Center, Im Neuenheimer Feld 280, 69120 Heidelberg, Germany

Frank Pianka and Sascha A. Müller
Department of General, Abdominal and Transplant Surgery, University of Heidelberg, Im Neuenheimer Feld 110, 69120 Heidelberg, Germany

Stefanie Satzl, Simone Schawo, and Boris Radeleff
Department of Radiology, University of Heidelberg, Im Neuenheimer Feld 110, 69120 Heidelberg, Germany

Ralf Tetzlaff
Division of Medical and Biological Informatics, and Department of Radiology, German Cancer Research Center, Im Neuenheimer Feld 280, 69120 Heidelberg, Germany

Alfred M. Franz
Division of Medical and Biological Informatics, German Cancer Research Center, Im Neuenheimer Feld 280, 69120 Heidelberg, Germany

Beat P. Müller-Stich
Department of General, Abdominal and Transplant Surgery, University of Heidelberg, Im Neuenheimer Feld 110, 69120 Heidelberg, Germany

I. Wolf
Division of Medical and Biological Informatics, German Cancer Research Center, Im Neuenheimer Feld 280, 69120 Heidelberg, Germany

H.-U. Kauczor
Department of Radiology, University of Heidelberg, Im Neuenheimer Feld 110, 69120 Heidelberg, Germany and Department of Radiology, German Cancer Research Center, Im Neuenheimer Feld 280, 69120 Heidelberg, Germany

B. M. Schmied
Department of General, Abdominal and Transplant Surgery, University of Heidelberg, Im Neuenheimer Feld 110, 69120 Heidelberg, Germany

H.-P. Meinzer
Division of Medical and Biological Informatics, German Cancer Research Center, Im Neuenheimer Feld 280, 69120 Heidelberg, Germany

(Received 27 May 2008; revised 25 August 2008; accepted for publication 27 September 2008; published 10 November 2008)

Computed tomography (CT)-guided percutaneous radiofrequency ablation (RFA) has become a commonly used procedure in the treatment of liver tumors. One of the main challenges related to the method is the exact placement of the instrument within the lesion. To address this issue, a system was developed for computer-assisted needle placement which uses a set of fiducial needles to compensate for organ motion in real time. The purpose of this study was to assess the accuracy of the system *in vivo*. Two medical experts with experience in CT-guided interventions and two nonexperts used the navigation system to perform 32 needle insertions into contrasted agar nodules injected into the livers of two ventilated swine. Skin-to-target path planning and real-time needle guidance were based on preinterventional 1 mm CT data slices. The lesions were hit in 97% of all trials with a mean user error of 2.4 ± 2.1 mm, a mean target registration error (TRE) of 2.1 ± 1.1 mm, and a mean overall targeting error of 3.7 ± 2.3 mm. The nonexperts achieved significantly better results than the experts with an overall error of 2.8 ± 1.4 mm ($n=16$) compared to 4.5 ± 2.7 mm ($n=16$). The mean time for performing four needle insertions based on one preinterventional planning CT was 57 ± 19 min with a mean setup time of 27 min, which includes the steps

 0094-2405/2008/35(12)/5385/12/$23.00 © 2008 Am. Assoc. Phys. Med.

fiducial insertion (24 ± 15 min), *planning CT acquisition* (1 ± 0 min), and *registration* (2 ± 1 min). The mean time for *path planning* and *targeting* was 5 ± 4 and 2 ± 1 min, respectively. Apart from the fiducial insertion step, experts and nonexperts performed comparably fast. It is concluded that the system allows for accurate needle placement into hepatic tumors based on one planning CT and could thus enable considerable improvement to the clinical treatment standard for RFA procedures and other CT-guided interventions in the liver. To support clinical application of the method, optimization of individual system modules to reduce intervention time is proposed. © *2008 American Association of Physicists in Medicine*. [DOI: 10.1118/1.3002315]

Key words: navigation, radiofrequency ablation, needle insertion, image-guided systems, motion compensation

I. INTRODUCTION

The liver is one of the most common sites for metastatic disease irrespective of the primary tumor. As many patients are not eligible for surgery, thermal ablation and especially radiofrequency ablation (RFA) emerges as an important additional therapy modality for the treatment of liver tumors.[1] One of the main challenges related to the intervention is the exact placement of the instrument, especially when the tumor is situated close to critical structures such as large vessels, the gall bladder, and the lungs. Radiofrequency needles can be placed under ultrasound (US), magnetic resonance (MR), or computed tomography (CT) guidance.[2] When sonographic placement is not possible (e.g., because the tumor is not visible in US images), CT is often the method of choice. In its original form, the procedure requires a preinterventional CT scan which is used to plan a trajectory to the target. The operator then has to "mentally" register the patient with the images to transfer the planned trajectory to the patient. Due to the lack of real-time imaging information this requires a lot of practice, especially when in-plane needle insertion is not possible. To lower the risk of needle misplacement, the needle position is checked repeatedly in control CT scans, leading to high radiation exposure for the patient and long procedure times. In addition, each correction increases the risk of tumor seeding and postprocedure complication. The introduction of CT fluoroscopy brought improvement through real-time feedback, but the physician's hand-eye coordination still remains a limiting factor and both the patient and the physician are exposed to additional doses of radiation.

Computer guidance appears to be a solution to the problem, but clinically available navigation systems have only been designed for rigid structures, such as the skull or the spine, where the target remains in a constant position relative to certain reference points. The liver, however, exhibits significant motion due to respiration.[3] To address this issue, several research groups (e.g., Refs. 4–9) are investigating methods for transferring established guidance concepts to soft tissue. The proposed approaches differ mainly in the following aspects (Table I):

(1) *Tracking method*: Most groups apply optical[6–8] and/or electromagnetic[5,6,9] systems to continuously locate surgical instruments during an intervention. Optical tracking systems are highly accurate but require a constant line-of-sight between the tracking system and the tracked sensors. Electromagnetic systems, on the other hand, are less robust but allow for integration of the sensors into the tip of an instrument.
(2) *Registration*: To visualize surgical instruments in relation to anatomical structures extracted from preinterventional images, it is necessary to register the tracking coordinate system with the image coordinate system. To achieve this, the most common approach is to construct fiducials that can be located by the tracking system and that are clearly visible in the CT images. Prior to the intervention these markers can be mounted onto the skin of the patient[5,6,8,9] and/or be inserted into the liver.[5,7]
(3) *Motion compensation*: The most common approach for compensating organ motion is to apply respiratory gating techniques, which are based on the assumption that the liver reoccupies the same position at identical points in the respiratory cycle. By performing the intervention in full expiration or inspiration only, the liver can be approximated as motionless. Alternatively (or additionally), a real-time deformation model can be applied, which estimates the position of a target structure continuously from the positions of tracked fiducials.[5,10]

Study design for *in vivo* accuracy assessment of guidance systems is challenging, and many different approaches have been investigated. Zhang *et al.*[5] injected contrasted agar nodules into the livers of two ventilated swine. The targeting error was determined from fluoroscopic images in anterior-posterior and lateral views. As these images were only two-dimensional, the target registration error (TRE) could not be determined with this approach. Fichtinger *et al.*[4] conducted experiments with ventilated swine cadavers and used stainless-steel staples as targets. The overall targeting error was determined from control CT scans. As the navigation system is based on 2D image overlay (the instruments are not tracked), there was no quantitative positional information throughout the procedure and the user error could thus not be determined. Kahn *et al.*[6] evaluated their navigation system using human cadavers, with three different targets: a predefined position within the ascending aorta, a calcified plaque in an artery, and the tip of a port catheter. The overall error was determined from control CT scans, but the user error and the TRE were not reported. Nicolau *et al.*[8] evaluated the system on six patients who underwent radio-

24734209, 2008, 12, Downloaded from https://aapm.onlinelibrary.wiley.com/doi/10.1118/1.3002315 by Hochschule Mannheim, Wiley Online Library on [24/08/2023]. See the Terms and Conditions (https://onlinelibrary.wiley.com/terms-and-conditions) on Wiley Online Library for rules of use; OA articles are governed by the applicable Creative Commons License

TABLE I. Selection of navigation approaches for computer-assisted needle placement in the liver.

Authors	Tracking method	Registration method	Motion compensation
Banovac *et al.* (Ref. 11)	Electromagnetic	Skin fiducials and fiducial needle	Gating
Fichtinger *et al.* (Ref. 4)	None (CT image overlay system)	Phantom for manually calibrating image overlay system with CT scanner	Gating
Khamene *et al.* (Ref. 22)	Electromagnetic, optical, and image-based (4D MRI for establishing correlation)	Plate equipped with magnetic and optical markers	Deformation model describing correlation between internal and external motion
Khan *et al.* (Ref. 6)	Optical (infrared, active) and electromagnetic	Skin fiducials	Gating
Krücker *et al.* (Ref. 9)	Electromagnetic	Skin fiducials, previous instrument positions	Gating, vacuum stabilization mattress
Maier-Hein *et al.* (Refs. 7 and 10)	Optical (infrared, passive)	Fiducial needles	Deformation model based on fiducial movement
Nagel *et al.* (Refs. 23 and 24)	Optical (infrared, passive) or electromagnetic	Reference frame (equipped with CT markers and optical/electromagnetic markers)	Gating, vacuum stabilization mattress
Nicolau *et al.* (Ref. 8)	Optical (color-based)	Skin fiducials	Gating
Schweikard *et al.* (Ref. 25)	Stereo x-ray and optical (infrared, active)	Internal gold markers and skin markers	Deformation model describing correlation between internal and external motion
Zhang *et al.* (Refs. 5 and 26)	Electromagnetic	Fiducial needles	Affine transformation based on fiducial movement

frequency ablation of the liver. The final position of the inserted instrument was ascertained from a control CT scan, which was registered rigidly with the planning CT image based on the segmented liver surfaces. Both the tracked needle position and the real needle position were transformed to the planning CT image, and the distance between the tips of the needles was defined as the system error. As the tracking information was not used to guide the needle placement, neither the user error nor the overall targeting error could be reported. Similarly, Krücker *et al.*[9] defined different anatomical targets in 19 patients and reported the tracking error as the distance between the virtual needle position superimposed onto the control CT image and the true needle position ascertained from the image. The registration of the planning CT image with the control CT image was based on surface markers serving as landmarks for a point-based registration. Again, the user error and the overall targeting error could not be reported because the navigation system had not been used to guide needle placement.

In a previous report,[7] we introduced a needle-based navigation system for minimally invasive interventions in the liver, in which a real-time deformation model is used to estimate the position of a navigation target point continuously from a set of optically tracked fiducial needles (Fig. 1). The overall targeting accuracy of the system was assessed *ex vivo* with a respiratory liver motion simulator and was 3.5 ± 1.1 mm on average. In this study, we assess the accuracy of our system *in vivo*. To be able to break down the overall error into individual components, we apply a modification of the approach proposed by Banovac *et al.*[11]

The remaining part of this article is organized as follows: First, we give a description of our navigation system and its core components in Sec. II A. Next, we present the study design (Secs. II B and II C), followed by the results (Sec. III) of our experiments. We end with a discussion (Sec. IV) and conclusions (Sec. V).

II. MATERIALS AND METHODS

II.A. Navigation system

Our navigation system estimates the position of an initially determined target structure continuously from a set of optically tracked fiducial needles (*navigation aids*). The workflow is illustrated in Fig. 1. Prior to the intervention, the navigation aids are inserted in the vicinity of the target. Next, a planning CT scan is acquired. The image coordinate system is then registered with the tracking coordinate system based on the fiducial positions (cf. *Registration*). Finally, a trajectory to the target is planned. During the intervention, the fiducial needles are continuously located by an optical tracking system and a real-time transformation is used to estimate the position of the target point accordingly (cf. *Deformation Model*). A suitable visualization scheme guides the physician towards the moving target (cf. *Visualization*). The software was implemented in the programming language C++ with the open-source toolkits *Insight Segmentation and Registration Toolkit* (ITK),[12] *The Visualization Toolkit* (VTK),[13] and *Medical Imaging Interaction Toolkit* (MITK).[14] In the following sections, we describe the core components of the system.

24734209, 2008, 12, Downloaded from https://aapm.onlinelibrary.wiley.com/doi/10.1118/1.3002315 by Hochschule Mannheim, Wiley Online Library on [24/08/2023]. See the Terms and Conditions (https://onlinelibrary.wiley.com/terms-and-conditions) on Wiley Online Library for rules of use; OA articles are governed by the applicable Creative Commons License

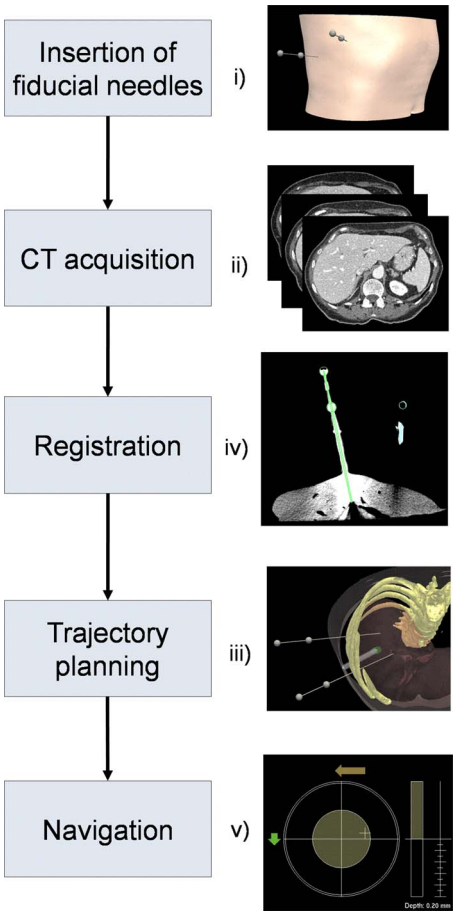

FIG. 1. Workflow for navigated needle placement.

II.A.1. Hardware

The navigation software runs on a Dell Precision M90 notebook (2 GHz dual-core processor, 2 GB RAM, NVIDIA FX 1500M graphics adapter) with an additional external monitor providing real-time visualization to the operator (Fig. 2). The Polaris optical tracking system [Northern Digital Inc. (NDI); Waterloo, Ontario, Canada] is used for tracking both the instrument and the fiducial needles. To obtain lightweight fiducial needles despite the minimal intermarker distance of 5 cm required by the manufacturer of the tracking system, we developed 5-Degrees-of-Freedom (5DoF) tools[15] with an arrangement of the optical markers along the axis of the tool (Fig. 3). To avoid needle deflection, we chose a needle radius of 1 mm. Custom-designed silicon patches, which provide high friction compared to porcine skin, are used to affix the needles to the skin and thus prevent them from slipping out. Note that the 5DoF tools must be constructed symmetrically because they cannot be calibrated: It is impossible to infer the position of the needle tip from the two markers if it is not located on the line defined by these markers. In a previous work[15] we have shown that we can construct the tools precisely and obtain submillimeter tracking accuracy.

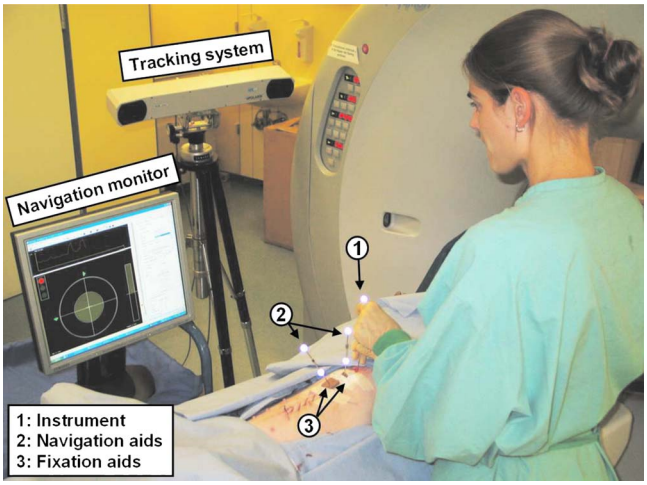

FIG. 2. Navigation system in the intervention room.

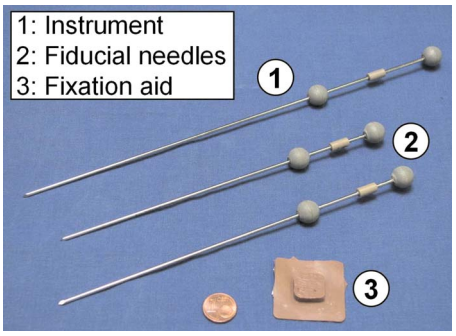

FIG. 3. Instrument (1) and navigation aids (2) with a needle radius of 1 mm and intermarker distances ranging from 45 to 75 mm. The fixation aid (3) is composed of silicon and prevents the fiducial needles from slipping out.

II.A.2. Registration

One of the main advantages of applying fiducial needles, as opposed to skin markers, for navigated needle placement is the fact that they allow reference points within the target organ itself to be used to register the tracking coordinate system with the CT coordinate system. To perform the registration, we have to locate the fiducials in both coordinate systems in matching states within the breathing cycle.

We propose a semiautomatic registration method based on the concept of model to image registration for locating the fiducial needles in the CT images. Each navigation aid is modeled by a composition of a cylinder (the needle) and two spheres (the markers), and can essentially be described by the needle length and the intermarker distance (the marker radius and the needle radius are the same for all tools). The parameters $\vec{p}$ to be optimized during the registration process represent a rigid transformation that maps the needle coordinate system onto the image coordinate system. To quantify the registration quality of the parameters $\vec{p}$ for a given needle model j, the model is transformed to a point cloud $P^j_1, \ldots, P^j_{N_j}$ and the following metric M is applied:

24734209, 2008, 12, Downloaded from https://aapm.onlinelibrary.wiley.com/doi/10.1118/1.3002315 by Hochschule Mannheim, Wiley Online Library on [24/08/2023]. See the Terms and Conditions (https://onlinelibrary.wiley.com/terms-and-conditions) on Wiley Online Library for rules of use; OA articles are governed by the applicable Creative Commons License

$$M(\vec{p},j)=\sum_{k=1}^{N_j} I(\Phi[\vec{p}](P_k^j)), \quad (1)$$

where $\Phi[\vec{p}]$ represents the rigid transformation defined by the parameters $\vec{p}$ and $I(P)$ returns the (linearly interpolated) pixel value in the CT image at point P. The metric is based on the assumption that the needles yield significantly higher Hounsfield values than the neighboring structures and air. It essentially sums up all voxel values inside the (moving) needle model.

To fit a needle into the image, the user identifies one (arbitrary) voxel P_{seed_i} on the needle within the image, and region growing is performed yielding a voxel cluster C_{needle_i}. Based on the center of mass of the voxel cluster C_{needle_i} and its orientation (principal component), an initial parameter set $\vec{p}_{\text{initial}}$ is computed. The needle model j yielding the best (initial) registration quality $M(\vec{p}_{\text{initial}},j)$ according to our metric is assumed to correspond to the given voxel cluster. Starting with the initial parameter set, a stochastic optimizer (itk::OnePlusOneEvolutionaryOptimizer[12]) is then used to maximize the metric value using a stochastic search algorithm. The final parameter set defines the position of the navigation aid j in image space. Note that we chose a stochastic optimizer, as opposed to a gradient-based optimizer, because it does not require the metric to be differentiable.

In the second stage of the registration procedure, we track the fiducial needles over time to identify the state within the breathing cycle at which the CT was taken. For this purpose, we extract two landmarks $\vec{l}_{j1}^{\,0},\vec{l}_{j2}^{\,0}$ from the axis of each registered fiducial needle j in image coordinates: the tip of the needle itself and a second point on the axis of the needle with a distance of 50 mm to the tip. The part of the needle defined by these two points is supposed to roughly represent the portion of the navigation aid that was inserted into the liver. We then track the fiducial needles over two breathing cycles, obtaining a sequence of tracked needle positions over time: $L^k=\{\vec{l}_{11}^{\,k},\vec{l}_{12}^{\,k},\vec{l}_{21}^{\,k},\vec{l}_{22}^{\,k}\}$. For each sample k we then compute a rigid transformation $\Phi_{k\to 0}$ mapping the current landmarks L^k onto the original landmarks L^0 based on the least-square method by Horn.[16] The coordinate transformation is then given by the transformation $\hat{\Phi}=\Phi_{\hat{k}\to 0}$ that minimizes the associated fiducial registration error (FRE),

$$\hat{k}=\arg\min_k \text{FRE}^k \quad (2)$$

$$\text{FRE}^k=\frac{1}{4}\sum_{j=1}^{2}\sum_{m=1}^{2}|\vec{l}_{jm}^{\,0}-\Phi_{k\to 0}(\vec{l}_{jm}^{\,k})|. \quad (3)$$

Note that this procedure enables us to automatically detect the state within the breathing cycle at which the CT was taken, and the patient can breathe freely as opposed to having to reproduce a certain respiratory state.

II.A.3. Motion compensation

In a previous report,[10] we assessed the target registration error (TRE) of our needle-based navigation system *in vitro* for different transformation types, numbers of fiducial needles, and placement strategies. Three needles yielded significantly better results than two over the breathing cycle, yet the results were similar for gated experiments. To reduce the invasiveness of the intervention, we chose to apply only two fiducial needles in this study and to conduct the intervention at expiration only, which allows us to approximate liver motion as rigid.

At the beginning of the intervention, a planning CT image is acquired, which is used to register the tracking coordinate system with the CT coordinate system as described above (cf. *Registration*). During the intervention itself, the system is updated every 100 ms. Each time, we extract a set of landmarks $L_{\text{track}}^{\text{cur}}$ from the tracked fiducial needle positions and transform them to image coordinates using $\hat{\Phi}$ (cf. *Registration*). Next, we compute a rigid transformation Φ_{cur} based on the least-squared method by Horn, which maps the original needle positions L^0 onto the transformed current positions $L_{\text{img}}^{\text{cur}}$. Finally, Φ_{cur} is used to transform the target point originally located in the planning CT,

$$\vec{t}_{\text{cur}}=\Phi_{\text{cur}}(\vec{t}_0). \quad (4)$$

Note that Φ_{cur} could readily be replaced by other real-time compatible transformations such as thin-plate splines or affine transformations.[10]

II.A.4. Visualization

The literature on visualization methods for navigated needle insertion is sparse. The majority of accuracy studies do not include a description of the user interface that was used to target a given anatomical structure. In a previous study, we compared several visualization schemes for guiding an operator to a predefined target.[17] Based on the results of that study, we developed a three-stage visualization scheme which consists of the following steps (Fig. 4): First, a projection view is provided for locating the planned insertion point on the skin of the patient. For this purpose, the tip of the instrument is projected onto the plane that passes the insertion point and that is orthogonal to the line connecting the insertion point and the target point. Once the insertion point is reached, the end of the instrument is projected onto the plane that passes the tip of the instrument and that is orthogonal to the line connecting the tip of the instrument and the target point. Finally, for the needle insertion process, we place a virtual camera into the tip of the instrument with its view direction along the needle axis. Additional structures visualize the depth of the instrument within the tissue.

II.B. Experimental conditions

This study was approved by the Committee for Animal Care and Research of the Karlsruhe regional council. Like Zhang *et al.*,[5] we assessed the accuracy of our navigation system by performing a total of 32 liver needle insertions in two 30 kg domestic swine (S1, S2) using hepatic agar nodules as artificial tumors. Two medical experts (E1, E2) with experience in CT-guided interventions (>50 punctures each)

24734209, 2008, 12, Downloaded from https://aapm.onlinelibrary.wiley.com/doi/10.1118/1.3002315 by Hochschule Mannheim, Wiley Online Library on [24/08/2023]. See the Terms and Conditions (https://onlinelibrary.wiley.com/terms-and-conditions) on Wiley Online Library for rules of use; OA articles are governed by the applicable Creative Commons License

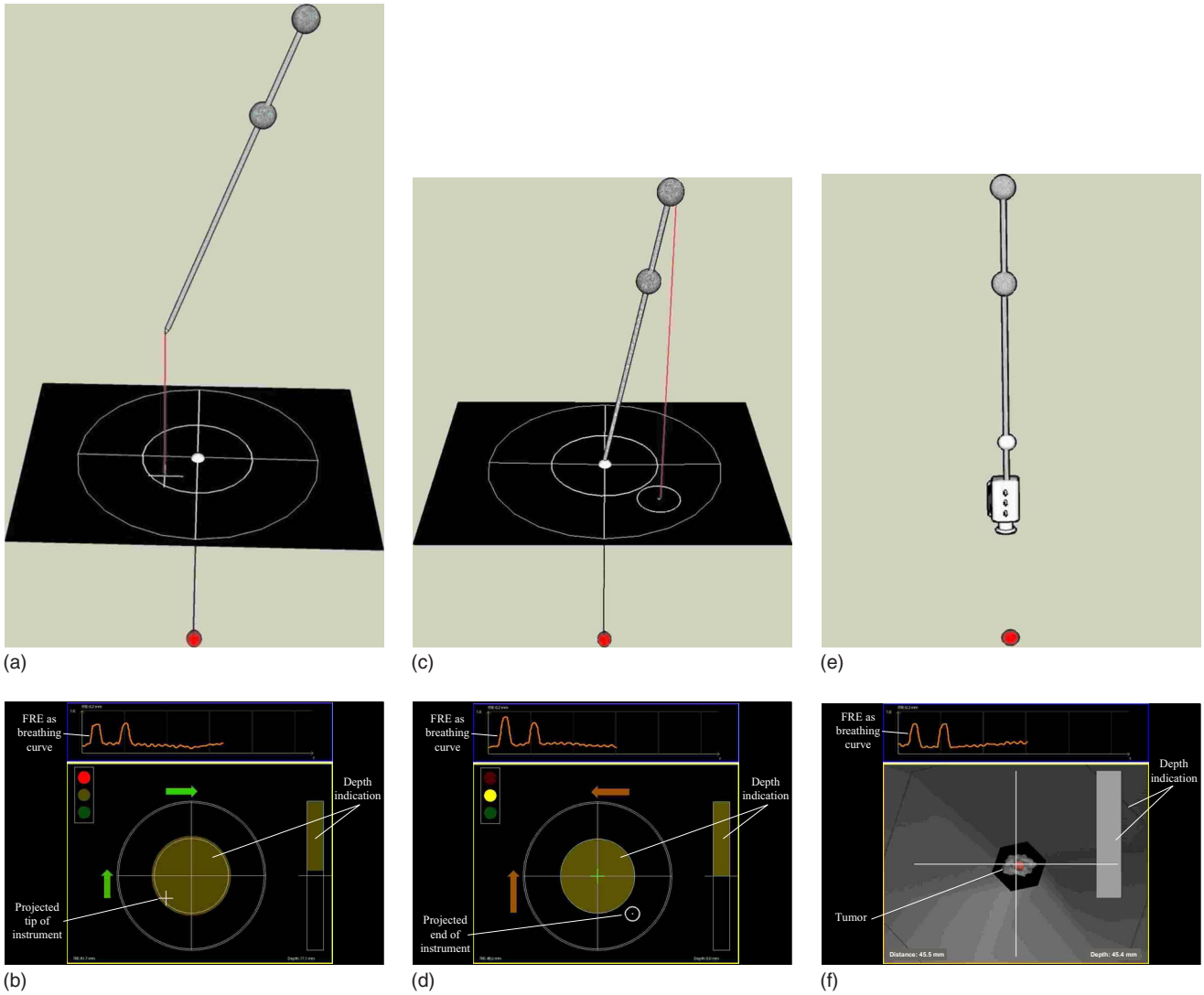

FIG. 4. Three-stage visualization scheme providing separate views for the steps *tip positioning*, *needle alignment*, and *needle insertion*. Schematic views (a,c,e) and corresponding screenshots (b,d,f).

and two fourth-year medical students, which we will refer to as nonexperts (NE1, NE2), performed eight interventions each. The following sections present the experimental conditions and describe the workflow in detail.

II.B.1. Animal preparation

Each animal was prepared for the intervention according to the following procedure. The swine was anesthetized, endotracheally intubated, and monitored throughout the experiments. A laparatomy was performed to inject four 2 ml agar nodules [5% agar dilution mixed with contrast agent (1:15 v/v dilution)] into the liver parenchyma using a 13 G venipuncture needle (cf. Tsuchida *et al.*[18]). Depending on the anatomy of the swine liver and the location of the incision, the nodules were injected either into the medial segment of the left hepatic lobe or into the medial segment of the right hepatic lobe, avoiding critical structures such as large vessels and the gall bladder. A CT scan of the abdomen confirmed the size and location of the sphere-shaped nodules (diameter: 1–2 cm). On completion of the experiments, the anesthetized animal was killed, using a venous injection of 2 mmol/kg potassium chloride to induce asystole.

II.B.2. Experimental workflow

In each swine, one expert and one nonexpert targeted each of the four lesions twice (two *passes*). For each pass, an ultrasound (US) device was used to insert the navigation aids such that they were arranged along the cranio-caudal axis of the animal and did not pass a lesion. Silicon patches (Fig. 3) were utilized to attach the needles firmly to the skin. Both operators then targeted the set of four lesions according to the following procedure. Preprocedural expiratory CT scans of the animal were acquired [Toshiba Aquilion 16 slice multidetector CT scanner (Toshiba, Tokyo, Japan); 1 mm slice thickness] showing the entire set of lesions and both navigation aids. Next, the navigation aid models were registered with the planning CT image according to the algorithm described in Sec. II A 2 (*Registration*). For each lesion, the

24734209, 2008, 12, Downloaded from https://aapm.onlinelibrary.wiley.com/doi/10.1118/1.3002315 by Hochschule Mannheim, Wiley Online Library on [24/08/2023]. See the Terms and Conditions (https://onlinelibrary.wiley.com/terms-and-conditions) on Wiley Online Library for rules of use; OA articles are governed by the applicable Creative Commons License

following workflow was then applied: First, a trajectory was planned. For this purpose, the lesion was segmented semiautomatically on the basis of the graph-cut algorithm.[19,20] A slice-based segmentation tool was then used to correct the tumor contours if necessary, and the navigation target point was set to the center of gravity of the segmented tumor. The operator chose an insertion point on the skin and the resulting path was visualized and—if necessary—modified. When path planning was complete, the tracking coordinate system was registered with the planning CT coordinate system as described in Sec. II A 2 (*Registration*). Guided by the navigation monitor (cf. Sec. II A 4, *Visualization*), the operator then used an optically tracked instrument (Fig. 3) to target the lesion. To obtain a minimal TRE (Ref. 10) and to facilitate the insertion process by keeping the target in a constant position,[21] the swine was held in expiration for 20 s intervals during the procedure. Once the operator was satisfied with the instrument position, a control CT scan was acquired with the same settings as for planning CT. Note that we used one fiducial needle configuration for both the expert and the nonexpert to obtain comparable experimental conditions. In S1, the nonexpert inserted the fiducial needles both times, and in S2, the expert inserted the needles. In all second passes, the lesions were targeted in reverse order. Tables IV and V list the experiments in chronological order.

II.C. Accuracy assessment

The majority of accuracy studies on guidance systems for needle punctures evaluate the overall targeting error, i.e., the distance between a reference target position and the final position of the tip of an inserted instrument in postprocedural images. Unfortunately, this error depends crucially on the provided visualization scheme and the experience of the user. To be able to quantify the contribution of different sources of error, we decided to additionally determine the user error and the TRE.

II.C.1. User error

The user error was defined as the distance between the tip of the instrument and the planned target point according to the navigation system prior to the control CT acquisition. The associated FRE of the applied transformation Φ_{cur} (cf. Sec. II A), which we will refer to as FRE^{user}, can be computed with Eq. (3).

II.C.2. TRE

The TRE, which is the distance between the true target position and the estimated target position, was approximated from the two CT images as follows: First, the fiducial needles were registered with the control CT image using the algorithm described in Sec. II A. Next, a set of landmarks was extracted from the registered needles (cf. Sec. II A 3, *Motion compensation*) and a point-based rigid registration of the two CT images was performed with these landmarks. The resulting rigid transformation $\Phi_{control}$ was then applied to transform the navigation target point t_0 computed in the planning CT scan to the control CT scan, and the TRE was defined as

$$\mathrm{TRE} = \left\| \vec{t}_{control} - \Phi_{control}(\vec{t}_0) \right\|, \quad (5)$$

where $t_{control}$ was the center of gravity of the segmented lesion in the control CT image. The associated FRE, which we will refer to as $FRE^{control}$, was also stored. Note that the true TRE originates from the tracked fiducial needles as opposed to the registered needle positions.

II.C.3. Overall error

The overall targeting error, or CT error, was defined as the distance between the tip of the inserted instrument and the center of gravity of the lesion in the control CT scan. To compute the error, the instrument model was registered to the control CT image with the semiautomatic approach described in Sec. II A, and the lesion was segmented semiautomatically with the graph-cut algorithm. [19]

The sources contributing to the individual errors as well as the limitations in computing the errors are given in Table II. Note that although the overall error can be approximated by the user error and the TRE, we cannot relate the individual components because they are computed on different images.

III. RESULTS

Our navigation system was applied for 32 needle insertions according to the workflow described above. The lesions were hit in 97% of all trials (31 out of 32) with a mean user error of 2.4 ± 2.1 mm, a mean TRE of 2.1 ± 1.1 mm, and a mean overall error of 3.7 ± 2.3 mm averaged over all trials (Table III). When the needle insertion was conducted immediately after the planning CT acquisition (first trial after CT acquisition), the TRE and the overall targeting error dropped to 1.7 ± 1.4 mm ($n=8$) and 2.3 ± 1.0 ($n=8$), respectively. The results of the individual trials are shown separately for the two swine in Tables IV and V, respectively. The nonexperts obtained better results than the medical experts with mean user errors of 1.6 ± 1.2 mm compared to 3.2 ± 2.4 mm. Figure 5 shows an example of an inserted instrument in a control CT scan.

The mean depth of the lesions within the tissue was 5 ± 3 cm, ranging from 1 to 11 cm. Despite the leverage effect, the targeting error did *not* increase with an increasing depth of the lesion, as shown in Fig. 6.

The mean RMS distance between the target and the control points on the fiducial needles in the planning CT scan was 6.2 ± 2.0 cm. The TRE did not correlate with the distance between the target and the fiducials. (Pearson product-moment correlation coefficient: 0.05).

The shift of the tumor relative to the navigation aids, which was computed from the registered images in the control CT coordinate system (cf. Sec. II C), occurred primarily in the anterior-posterior direction, which corresponds to the *y*-axis of the image coordinate system. An example is shown in Fig. 7. Similarly, the direction of the error vector measured in the control CT scan was not (necessarily) along the

24734209, 2008, 12, Downloaded from https://aapm.onlinelibrary.wiley.com/doi/10.1118/1.3002315 by Hochschule Mannheim, Wiley Online Library on [24/08/2023]. See the Terms and Conditions (https://onlinelibrary.wiley.com/terms-and-conditions) on Wiley Online Library for rules of use; OA articles are governed by the applicable Creative Commons License

TABLE II. Sources of the user error, the TRE, and the overall error defined in Sec. II C and limitations in computing these errors.

	Sources	Limitations
User error		—
	• Initial alignment error (cannot be corrected after partial insertion)	
	• Erroneous instrument geometry	
	• No fixation of instrument	
TRE		
	• Inaccurate registration of fiducial needles in planning CT scan	• Inaccurate lesion segmentation
	• Tumor shift due to instrument insertion	• Contrast agent (for locating lesions) diminishes over time
	• Tissue deformation	• Registered needles as opposed to tracked needles are used to estimate the target position
	• Bad fixation of fiducial needles	
	• Deflection of fiducials	
	• Inaccurate reproduction of the expiratory state	
Overall error		
	• User error (see above)	• Inaccurate registration of the instrument to the control CT scan (e.g. due to oscillation of the tool during image acquisition)
	• TRE (see above)	
	• Tool tracking error	
	• Instrument deflection	• Inaccurate lesion segmentation
		• Contrast agent (for locating lesions) diminishes over time

needle axis but also in the anterior-posterior direction with a mean y-component of +1.9 mm, reflecting a shift downwards.

The mean time for performing four needle insertions based on one planning CT (i.e., for one pass) was 57 ± 19 min with a mean setup time of 27 min, which comprises the times for *fiducial insertion* (24 ± 15 min), *planning CT acquisition* (1 ± 0 min), and *registration* (2 ± 1 min). The mean time for path planning and targeting was 5 ± 4 and 2 ± 1 min, respectively. Apart from the fiducial insertion step, experts and nonexperts obtained comparable results (Table VI).

IV. DISCUSSION

Although RFA has become a commonly used procedure in the treatment of liver tumors, it has several technical limitations which are mostly related to the difficulty of precisely positioning the instrument within the lesion to achieve adequate margins. To improve the procedure, we proposed a system for computer-assisted needle placement which uses a set of fiducial needles to compensate for organ motion in real time. In this study, we assessed the accuracy of our system and obtained a mean user error of 2.4 ± 2.1 mm, a TRE of 2.1 ± 1.1 mm, and an overall targeting error of 3.7 ± 2.3 mm averaged over 32 needle insertions performed by four operators in two swine. By breaking the overall error down into multiple components we were able to quantify the contribution of different error sources.

The proposed needle placement approach has several major advantages compared to the conventional CT-guided method. First, accurate needle placement can be achieved with only one planning CT scan, leading to low radiation exposure for the patient. As the targeting error does not increase with increasing tumor depth, the system can be used for targeting small lesions that are located deep within the tissue. Finally, in-plane instrument insertion is not required, because the system is based on 3D imaging data.

According to Table VII, our system is highly accurate in comparison with related work. We attribute this mainly to the application of needle-shaped fiducials for registration and

TABLE III. Error statistics computed on the entire set of 32 trials according to the definitions in Sec. II C.

	TRE [mm]	$FRE^{control}$ [mm]	User error [mm]	FRE^{user} [mm]	Overall error [mm]
Mean	2.1	0.7	2.4	0.9	3.7
SD	1.1	0.4	2.1	0.4	2.3
RMS	2.4	0.8	3.1	0.9	4.3
Median	1.9	0.6	1.7	0.7	3.4
Max	5.4	1.9	11.0	1.7	11.6

24734209, 2008, 12, Downloaded from https://aapm.onlinelibrary.wiley.com/doi/10.1118/1.3002315 by Hochschule Mannheim, Wiley Online Library on [24/08/2023]. See the Terms and Conditions (https://onlinelibrary.wiley.com/terms-and-conditions) on Wiley Online Library for rules of use; OA articles are governed by the applicable Creative Commons License

TABLE IV. TRE with corresponding FRE, user error with corresponding FRE, and overall targeting error (all in mm) as defined in Sec. II C for the individual trials (Lx: lesion ID) of expert 1 (E1) and nonexpert 1 (NE1) in swine 1 (S1). The mean errors (± standard deviation) for the experts, the nonexperts, and all operators are also reported.

	TRE [mm]	$FRE^{control}$ [mm]	User error [mm]	FRE^{user} [mm]	Overall error [mm]
NE1, pass 1					
L1	0.6	0.3	0.7	0.9	1.0
L2	2.0	0.6	3.3	1.2	6.1
L3	2.7	0.4	0.9	0.8	3.3
L4	3.7	1.6	1.2	1.6	4.4
E1, pass 1					
L1	1.2	0.4	4.6	0.7	5.8
L2	1.4	0.8	3.4	1.1	6.1
L3	2.9	0.3	4.4	0.7	3.8
L4	1.8	0.9	2.0	1.7	3.4
NE1, pass 2					
L4	2.4	0.5	1.7	1.1	2.9
L3	1.5	0.6	1.5	0.8	3.4
L2	3.2	0.9	3.9	0.6	3.8
L1	3.3	0.9	3.1	1.3	3.2
E1, pass 2					
L4	2.3	0.7	4.7	0.6	5.0
L3	1.7	0.3	4.1	0.4	6.3
L2	2.4	0.9	11.0	0.6	11.6
L1	2.2	0.4	3.3	0.6	5.2
Expert	2.0 ± 0.6	0.6 ± 0.3	4.7 ± 2.7	0.8 ± 0.4	5.9 ± 2.5
Nonexpert	2.4 ± 1.0	0.7 ± 0.4	2.0 ± 1.2	1.0 ± 0.3	3.5 ± 1.4
Both	2.2 ± 0.8	0.7 ± 0.4	3.4 ± 2.5	0.9 ± 0.4	4.7 ± 2.3

motion compensation. Furthermore, we use optical tracking, which is known to be considerably more accurate than electromagnetic tracking. We also believe that we obtain a comparatively low user error—unfortunately, it has not been reported in other studies (Table VII).

One purpose of this study was to assess the contribution of different error sources to the overall targeting error. To achieve this, we applied a modification of the approach proposed by Zhang *et al.*[5] using control CT scans for instrument verification as opposed to 2D fluoroscopic images. To our knowledge, we are the first to provide a detailed error analysis. A limitation of our evaluation approach, on the other hand, is the lack of fixation of the instrument within the lesion. In fact, all participants in this study reported a shift of the instrument once they released it to allow for the control CT scan acquisition, which led to a relatively large user error (and thus overall error) in several cases. Despite the fact that the operators were allowed to reposition the instrument until they were satisfied with the result, optimal positioning was not always possible due to the weight of the instrument, which tended to pull the needle partly out of the liver when the trajectory was short. One lesion (S1, L2), for instance, was situated so close to the liver capsule that the instrument did not even stay within the liver parenchyma, which led to high user errors of up to 12 mm. Note that this phenomenon is a possible explanation for the fact that we generally did not obtain higher accuracy for short trajectories: The deeper the lesion, the better the fixation of the needle. Unfortunately, the anatomy of the porcine livers did not always allow for implantation of deeply located lesions. We considered anchoring the instrument within the liver itself, yet the soft tissue anchor would have potentially destroyed the lesion and thus not have allowed multiple needle insertions. We are aware of the fact that needle movement is generally a problem for both conventional and computer-assisted needle insertions; however, it has not been discussed in related studies.

Surprisingly, the nonexperts performed better than the experts, with a user error of 1.6 ± 1.2 mm compared to 3.2 ± 2.4 mm. A possible explanation for this phenomenon is the fact that the experts are accustomed to inserting the needle very quickly. The nonexperts, on the other hand, had to learn the procedure without any prior knowledge and were thus more amenable to the navigated method. We plan to investigate this issue in the future.

Although we performed gated experiments, the TRE was significantly larger than zero, indicating tumor shift and/or deformation that was not captured by the fiducials. We attribute this mainly to the manipulation of the tissue by repeated needle insertions, because needle insertions that were conducted immediately after the planning CT acquisition yielded better accuracy than the remaining ones. Furthermore, the instrument was reused many times and thus potentially caused more tissue deformation than a sharp needle would have caused. Registration of the planning CT scan with the control CT scan showed that the tumor shifted pri-

24734209, 2008, 12, Downloaded from https://aapm.onlinelibrary.wiley.com/doi/10.1118/1.3002315 by Hochschule Mannheim, Wiley Online Library on [24/08/2023]. See the Terms and Conditions (https://onlinelibrary.wiley.com/terms-and-conditions) on Wiley Online Library for rules of use; OA articles are governed by the applicable Creative Commons License

TABLE V. TRE with corresponding FRE, user error with corresponding FRE, and overall targeting error (all in mm) as defined in Sec. II C for the individual trials (Lx: lesion ID) of the expert 2 (E2) and nonexpert 2 (NE2) in swine 2 (S2). The mean errors (± standard deviation) for the experts, the nonexperts, and all operators are also reported.

	TRE [mm]	$FRE^{control}$ [mm]	User error [mm]	FRE^{user} [mm]	Overall error [mm]
E2, pass 1					
L1	3.0	1.3	2.1	1.2	0.6
L2	1.8	0.9	2.6	1.4	3.3
L3	4.1	1.6	2.1	1.5	3.7
L4	5.4	1.9	0.9	1.4	7.1
NE2, pass 1					
L1	1.2	0.3	0.6	0.6	0.9
L2	1.5	0.6	3.7	0.4	2.7
L3	1.3	0.6	0.9	0.5	2.2
L4	1.9	0.6	0.9	0.7	3.0
E2, pass 2					
L4	1.0	0.2	1.8	0.3	0.7
L3	0.6	0.2	1.3	0.5	2.5
L2	1.7	0.6	1.7	0.6	3.9
L1	0.9	0.8	1.6	0.5	2.9
NE2, pass 2					
L4	1.5	0.7	1.0	0.7	1.8
L3	0.5	1.1	0.9	1.1	1.6
L2	2.8	0.8	0.8	0.9	0.7
L1	2.5	0.5	0.5	0.8	3.9
Expert	2.3 ± 1.7	0.9 ± 0.6	1.7 ± 0.5	0.9 ± 0.5	3.1 ± 2.1
Nonexpert	1.6 ± 0.7	0.7 ± 0.2	1.2 ± 1.0	0.7 ± 0.2	2.1 ± 1.1
Both	2.0 ± 1.3	0.8 ± 0.5	1.5 ± 0.8	0.8 ± 0.4	2.6 ± 1.7

marily in the anterior-posterior direction—not (necessarily) along the direction of the instrument. This displacement could possibly have been captured by the fiducial needles if they had been affixed within the liver itself and not on the skin, which, however, would have raised new issues in the context of tool design and risk of injury.

If measured over the entire breathing cycle, the TRE depends crucially on the applied deformation model as well as on the placement of the fiducial needles.[10] In gated experiments, on the other hand, the increase in error caused by suboptimal fiducial placement is relatively small compared to the overall TRE. This is a possible explanation for the fact that the TRE did not correlate with the distance between the target and the navigation aids in our experiments.

The operators performed four needle insertions based on only one planning CT, reflecting the fact that needle repositioning is very common during RFA procedures to completely destroy a tumor. When the needle insertion was conducted immediately after the planning CT acquisition, the error dropped significantly. Therefore, the trade-off between accuracy and time should be considered when deciding on an optimal number of planning CTs in practice.

The time for inserting the fiducial needles via ultrasound was relatively long (24 min), especially for the nonexperts (33 min) who had no experience in punctures. This can partly be attributed to the fact that the operators were not familiar with the anatomy of the swine. Furthermore, one fiducial needle configuration was used for targeting all four lesions, which had to be considered when planning the fiducial insertion. Still, intervention time was not the focus of this report. In an ongoing study, we compare the conventional biopsy method with our navigated approach and have so far obtained an average procedure time of the order of magnitude of 20 min ($n=20$) for tumor biopsies in swine with our navigation system. We are confident that the duration can be further decreased with increasing experience of the operator.

The majority of studies on navigation systems for soft tissue do not include a description of the user interface that is used to guide the operator. In this article, we presented a novel three-stage visualization scheme which allows for fast targeting of anatomical structures with a needle-shaped instrument. The approach is extremely popular among our

TABLE VI. Mean duration (± standard deviation) in min of the individual steps of the navigation workflow for the experts, the nonexperts, and averaged over all operators.

	Experts	Nonexperts	All
Fiducial insertion	14 ± 5	33 ± 16	24 ± 15
Planning-CT	1 ± 0	1 ± 0	1 ± 0
Registration	2 ± 1	2 ± 1	2 ± 1
Path planning	5 ± 3	5 ± 4	5 ± 4
Targeting	2 ± 1	2 ± 1	2 ± 1

24734209, 2008, 12, Downloaded from https://aapm.onlinelibrary.wiley.com/doi/10.1118/1.3002315 by Hochschule Mannheim, Wiley Online Library on [24/08/2023]. See the Terms and Conditions (https://onlinelibrary.wiley.com/terms-and-conditions) on Wiley Online Library for rules of use; OA articles are governed by the applicable Creative Commons License

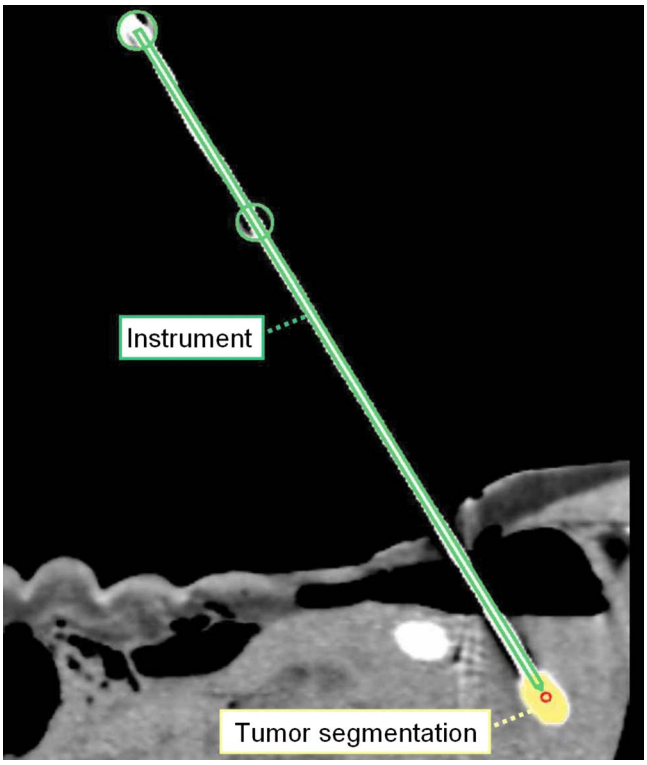

FIG. 5. Control CT scan showing the registered instrument, the segmented lesion within the liver, and the center of gravity of the lesion.

clinical partners and we consider it an important contribution to the field of image-guided systems.

Several issues remain to be addressed. First, the system needs to be tested under all possible clinical conditions. The experiments in this study were conducted with ventilated swine, but several interventions are conducted under local anesthesia with the patient breathing freely. Second, the lesions were targeted based on only one planning CT, leading to low radiation exposure for the patient. In practice, however, it might be useful to control the needle position with a second CT scan prior to performing the ablation or the biopsy. This way, high targeting errors (outliers) could be avoided. Finally, the insertion of the fiducial needles initially increased the invasiveness of the intervention. Although this is compensated by the high accuracy of the system, which reduces the risk of repeated instrument insertions, we are currently investigating replacing one of the fiducial needles with a set of skin markers for motion compensation. As fiducial insertion is one of the most time-consuming steps within the workflow, this could reduce intervention time significantly. Furthermore, we consider application of an electromagnetic tracking system, which would allow the integration of the sensors into the needle tips. Consequently, needle deflections would no longer be an issue and we could use thinner needles.

V. CONCLUSIONS

Our liver navigation system allowed for accurate needle placement into hepatic tumors with ventilated swine based on only one planning CT scan. Due to its low targeting error, which did not increase with increasing depth of the target, the system allows the targeting of small lesions as well as of lesions located deep within the tissue. As the system is based on 3D imaging data, it does not require in-plane instrument insertion. The high accuracy could potentially eliminate the need for repeated needle insertions and thus lead to lower complication rates such as hemorrhages and also reduce the patient's exposure to radiation. Taking these aspects into account, we believe that our navigation approach could potentially enable considerable improvement to the clinical treatment standard for RFA procedures and other CT-guided interventions in the liver. To support clinical application of our method, we propose the optimization of individual system modules with the goal of reducing the intervention time.

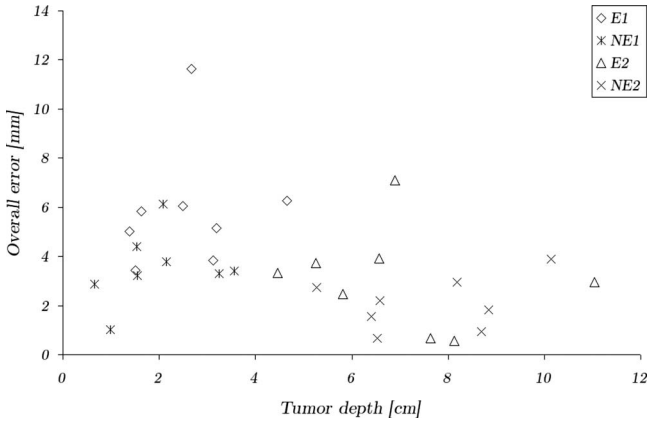

FIG. 6. Overall targeting error plotted against tumor depth.

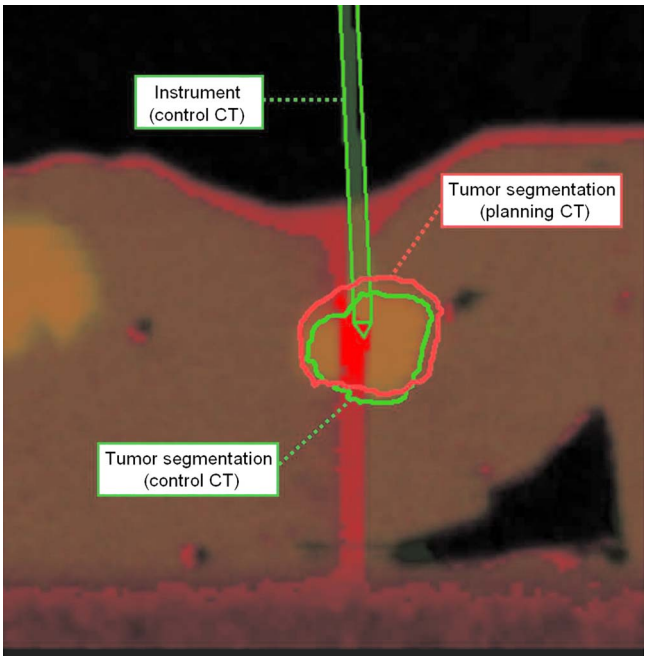

FIG. 7. Planning CT image registered to the control CT image showing the shift of the tumor due to instrument insertion. The segmentation of the lesions are shown as contours for the planning CT image and the control CT image, respectively.

24734209, 2008, 12, Downloaded from https://aapm.onlinelibrary.wiley.com/doi/10.1118/1.3002315 by Hochschule Mannheim, Wiley Online Library on [24/08/2023]. See the Terms and Conditions (https://onlinelibrary.wiley.com/terms-and-conditions) on Wiley Online Library for rules of use; OA articles are governed by the applicable Creative Commons License

TABLE VII. Selection of *in vivo* accuracy studies for computer-assisted needle placement in the liver. All errors are given in mm (mean ± standard deviation). SM: skin marker, FN: fiducial needle, PIP: previous instrument position. For Krücker *et al.* (Ref. 9) the system error represents the error which the authors referred to as tracking error (cf. Sec. IV). Banovac *et al.* (Ref. 11) reported the median as opposed to the mean targeting error.

Authors	Fiducials	Trials	System error	TRE	User error	Overall error
Banovac *et al.* (Ref. 11)	4 SM, 1 FN	$n=32$	—	—	—	8.3 ± 3.7
Fichtinger *et al.* (Ref. 4)	—	$n=22$	—	—	—	6.4 ± 1.8
Khan *et al.* (Ref. 6)	9 SM	$n=42$	—	—	—	8.4 ± 1.8
Krücker *et al.* (Ref. 9)	5-7 SM	$n=61$	5.8 ± 2.6	—	—	—
Krücker *et al.* (Ref. 9)	5-7 SM, 1-8 PIP	$n=59$	3.5 ± 1.9	—	—	—
Maier-Hein *et al.*	2 FN	$n=32$	—	2.1 ± 1.1	2.4 ± 2.1	3.7 ± 2.3
Nicolau *et al.* (Ref. 8)	6-15 SM	$n=6$	$4.3 \pm$ n/a	—	—	—

ACKNOWLEDGMENTS

The present study was conducted within the setting of "Research training group 1126: Intelligent Surgery—Development of new computer-based methods for the future workplace in surgery" funded by the German Research Foundation (DFG).

[a]Electronic mail: l.maier-hein@dkfz.de

[1]P. L. Pereira, "Actual role of radiofrequency ablation of liver metastases," Eur. Radiol. **17**(8), 2062–2070 (2007).
[2]J. P. McGahan and G. D. Dodd, "Radiofrequency ablation of the liver: Current status," AJR, Am. J. Roentgenol. **176**(1), 3–16 (2001).
[3]M. A. Clifford, F. Banovac, E. Levy, and K. Cleary, "Assessment of hepatic motion secondary to respiration for computer assisted interventions," Comput. Aided Surg. **7**(5), 291–299 (2002).
[4]G. Fichtinger, A. Deguet, G. Fischer, I. Iordachita, E. Balogh, K. Masamune, R. H. Taylor, L. M. Fayad, M. de Oliveira, and S. J. Zinreich, "Image overlay for CT-guided needle insertions," Comput. Aided Surg. **10**(4), 241–255 (2005).
[5]H. Zhang, F. Banovac, R. Lin, N. Glossop, B. J. Wood, D. Lindisch, E. Levy, and K. Cleary, "Electromagnetic tracking for abdominal interventions in computer aided surgery," Comput. Aided Surg. **11**(3), 127–136 (2006).
[6]M. F. Khan, S. Dogan, A. Maataoui, S. Wesarg, J. Gurung, H. Ackermann, M. Schiemann, G. Wimmer-Greinecker, and T. J. Vogl, "Navigation-based needle puncture of a cadaver using a hybrid tracking navigational system," Invest. Radiol. **41**(10), 713–720 (2006).
[7]L. Maier-Hein, F. Pianka, A. Seitel, S. A. Müller, A. Tekbas, M. Seitel, I. Wolf, B. M. Schmied, and H.-P. Meinzer, "Precision targeting of liver lesions with a needle-based soft tissue navigation system," in *Proceedings of the 10th International Conference on Medical Image Computing and Computer-Assisted Intervention—MICCAI 2007 (2)*, edited by N. Ayache *et al.* (Springer, Brisbane, Australia, October 2007), Vol. 4792, pp. 42–49.
[8]S. A. Nicolau, X. Pennec, L. Soler, and N. Ayache, "Clinical evaluation of a respiratory gated guidance system for liver punctures," in Ref. 7, pp. 77–85 (Springer, Brisbane, Australia, October 2007).
[9]J. Krücker, S. Xu, N. Glossop, A. Viswanathan, J. Borgert, H. Schulz, and B. J. Wood, "Electromagnetic tracking for thermal ablation and biopsy guidance: Clinical evaluation of spatial accuracy," J. Vasc. Interv. Radiol. **18**(9), 1141–1150 (2007).
[10]L. Maier-Hein, S. A. Müller, F. Pianka, S. Wörz, B. P. Müller-Stich, A. Seitel, K. Rohr, H.-P. Meinzer, B. Schmied, and I. Wolf, "Respiratory motion compensation for CT-guided interventions in the liver," Comput. Aided Surg. **13**(3), 125–138 (2008).
[11]F. Banovac, J. Tang, S. Xu, D. Lindisch, H. Y. Chung, E. Levy, T. Chang, M. F. McCullough, Z. Yaniv, B. J. Wood, and K. Cleary, "Precision targeting of liver lesions using a novel electromagnetic navigation device in physiologic phantom and swine," Med. Phys. **32**(8), 2698–2705 (2005).
[12]L. Ibañez, W. Schroeder, L. Ng, and J. Cates, and the Insight Software Consortium, *The ITK Software Guide Second Edition*, 2005. http://www.itk.org.
[13]W. J. Schroeder, K. M. Martin, L. S. Avila, and C. C. Law, *The Visualization Toolkit User's Guide*, August 2003.
[14]I. Wolf, M. Vetter, I. Wegner, T. Böttger, M. Nolden, M. Schöbinger, M. Hastenteufel, T. Kunert, and H.-P. Meinzer, "The Medical Imaging Interaction Toolkit," Med. Image Anal. **9**(6), 594–604 (2005).
[15]L. Maier-Hein, D. Maleike, J. Neuhaus, A. Franz, I. Wolf, and H.-P. Meinzer, "Soft tissue navigation using needle-shaped markers: Evaluation of navigation aid tracking accuracy and CT registration," in *Proceedings of SPIE Medical Imaging 2007: Visualization, Image-Guided Procedures, and Display*, edited by K. R. Cleary and M. I. Miga, February 2007, Vol. 6509, p. 650926.
[16]B. Horn, "Closed-form solution of absolute orientation using unit quaternions," J. Opt. Soc. Am. A **4**, 629–642 (1987).
[17]A. Seitel, L. Maier-Hein, S. Schawo, B. A. Radeleff, S. A. Müller, F. Pianka, B. M. Schmied, I. Wolf, and H.-P. Meinzer, "In-vitro evaluation of different visualization approaches for computer assisted targeting in soft tissue," in *Int J CARS 2 (Suppl 1)*, pp. 188–190 (Springer, Berlin, 2007).
[18]M. Tsuchida, Y. Yamato, T. Aoki, T. Watanabe, N. Koizumi, I. Emura, and J. Hayashi, "CT-guided agar marking for localization of nonpalpable peripheral pulmonary lesions," Chest **116**(1), 139–143 (1999).
[19]Y. Boykov and V. Kolmogorov, "An experimental comparison of min-cut/max-flow algorithms for energy minimization in vision," IEEE Trans. Pattern Anal. Mach. Intell. **26**(9), 1124–1137 (2004).
[20]M. Linkenheil, "Graph-Cut-Segmentierung für die medizinische Bildverarbeitung," Master's thesis, German Cancer Research Center, Div. Medical and Biological Informatics, 2005.
[21]J. M. Balter, K. L. Lam, C. J. McGinn, T. S. Lawrence, and R. K. Ten Haken, "Improvement of CT-based treatment-planning models of abdominal targets using static exhale imaging," Int. J. Radiat. Oncol., Biol., Phys. **41**(4), 939–943 (1998).
[22]A. Khamene, J. K. Warzelhan, S. Vogt, D. Elgort, C. Chefd'Hotel, J. L. Duerk, J. S. Lewin, F. K. Wacker, and F. Sauer, "Characterization of internal organ motion using skin marker positions," in *Proceedings of the 7th International Conference on Medical Image Computing and Computer-Assisted Intervention - MICCAI 2004 (2)*, edited by C. Barillot, D. R. Haynor, and P. Hellier (Springer, Saint-Malo, France, 2004), pp. 526–533.
[23]M. Nagel, G. Schmidt, R. Petzold, and W. A. Kalender, "A navigation system for minimally invasive CT-guided interventions," in *Proceedings of the 8th International Conference on Medical Image Computing and Computer-Assisted Intervention - MICCAI 2005 (2)*, edited by J. S. Duncan and G. Gerig (Springer, Palm Springs, CA, 2005), pp. 33–40.
[24]M. Nagel, M. Hoheisel, R. Petzold, W. A. Kalender, and U. H. W. Krause, "Needle and catheter navigation using electromagnetic tracking for computer-assisted C-arm CT interventions," in *Proceedings of SPIE Medical Imaging 2007: Visualization, Image-Guided Procedures, and Display*, edited by K. R. Cleary and M. I. Miga San Diego, CA, February 2007, Vol. 6509, p. 65090J.
[25]A. Schweikard, G. Glosser, M. Bodduluri, M. J. Murphy, and J. R. Adler, "Robotic motion compensation for respiratory movement during radiosurgery," Comput. Aided Surg. **5**, 263–277 (2000).
[26]H. Zhang, F. Banovac, N. D. Glossop, and K. Cleary, "Two-stage registration for real-time deformable compensation using an electromagnetic tracking device," in Ref. 23, pp. 992–999.

24734209, 2008, 12, Downloaded from https://aapm.onlinelibrary.wiley.com/doi/10.1118/1.3002315 by Hochschule Mannheim, Wiley Online Library on [24/08/2023]. See the Terms and Conditions (https://onlinelibrary.wiley.com/terms-and-conditions) on Wiley Online Library for rules of use; OA articles are governed by the applicable Creative Commons License